

# Mixing properties of phengitic micas and revised garnet-phengite thermobarometers

R. COGGON AND T. J. B. HOLLAND

*University of Cambridge, Department of Earth Sciences, Downing Street, Cambridge CB2 3EQ, UK*  
(tjbh@esc.cam.ac.uk)

**ABSTRACT** Mixing properties for muscovite–celadonite–ferroceladonite solid solutions are derived from combining available experimental phase equilibrium data with tabulated thermodynamic data for mineral end-members. When a partially ordered solution model is assumed, the enthalpy of mixing among the end-members muscovite–celadonite–ferroceladonite is nearly ideal, although the Gibbs energies of muscovite–celadonite and muscovite–ferroceladonite solutions are asymmetric due to an asymmetry in the entropy of mixing. Thermodynamic consistency is achieved for data on phengite compositions in assemblages with (a) pyrope + kyanite + quartz/coesite (b) almandine + kyanite + quartz/coesite (c) talc + kyanite + quartz/coesite and (d) garnet–phengite pairs equilibrated both experimentally at high temperatures and natural pairs from low-grade schists. The muscovite–paragonite solvus has been reanalysed using the asymmetric van Laar model, and the effects of the phengite substitution into muscovite have been quantitatively addressed in order to complete the simple thermodynamic mixing model for the solid solution among the mica end-members. Results are applied to a natural pyrope–coesite–phengite–talc rock from the Western Alps, and to investigate the conditions under which biotite-bearing mica schists transform to whiteschist-like biotite-absent assemblages for average pelite bulk compositions.

## INTRODUCTION

White mica has long been known to become increasingly phengitic with rising pressure in regional metamorphism (Ernst, 1963); this was experimentally verified by Velde (1965) who also recognised the potential for a geobarometer. Powell & Evans (1983) used Velde's limited experimental compositions with approximate entropy and volume data for the celadonite end-member to define the first thermodynamically defined phengite barometer. Since then two parallel developments have occurred: first, much more experimental work on phengite composition, as a function of  $P$ ,  $T$  and bulk composition, has become available (Massonne & Schreyer, 1986, 1987, 1989; Massonne & Szpurka, 1997) and second, the quality of thermodynamic data for minerals has reached a point where reliably precise estimates may be made for the thermodynamic properties of end-members, such as celadonite, that may be experimentally or naturally unstable. Since the experiments of Massonne & Schreyer (1989) it has been possible to determine crude thermodynamic data for Mg-celadonite, although this required some assumptions and interpolations to estimate equilibrium talc compositions (Al contents) in order to do this (Holland & Powell, 1998). These data were shown to be in broad agreement with the experiments of Massonne & Schreyer (1987) on K-feldspar + phlogopite + phengite + quartz assemblages if crude assumptions about compositions of the coexisting aluminous phlogopites

were also made. More recently it has become clear from the studies of white mica compositions by Vidal and co-workers (e.g. Agard *et al.*, 2001; Vidal & Parra, 2000; Trotet *et al.*, 2001) that an important mechanism leading to cation interlayer deficiency in white micas may be caused by introduction of a pyrophyllite substitution. The thermodynamic consequences of this will be explored further, in the applications section.

In this study the thermodynamic properties of minerals from the internally consistent compilation of Holland & Powell (1998) are used together with known and estimated properties of celadonite and ferroceladonite end-members and the most recent experimental data to derive a consistent set of thermodynamic data for micas in the model system muscovite (mu,  $\text{KAl}_3\text{Si}_3\text{O}_{10}(\text{OH})_2$ )–celadonite (cel,  $\text{KMgAlSi}_4\text{O}_{10}(\text{OH})_2$ )–ferroceladonite (fcel,  $\text{KFeAlSi}_4\text{O}_{10}(\text{OH})_2$ )–paragonite (pa,  $\text{NaAl}_3\text{Si}_3\text{O}_{10}(\text{OH})_2$ ). Note that the term celadonite used in this study refers to the phengite end-member and should not be confused with the naturally occurring mineral of that name formed in low temperature environments.

The experiments of Massonne & Szpurka (1997) became available after preparation of the celadonite thermodynamic data in the publication of Holland & Powell (1998). These experiments involved equilibration of phengite with garnet, kyanite and quartz (or coesite) in two chemical subsystems, KMASH and KFLASH, enabling the thermodynamic properties for both celadonite and ferroceladonite to be derived

without assumptions about compositions of coexisting biotite. Massonne & Szpurka made such an analysis and concluded that the phengite solid solution was non-ideal and asymmetric in its properties. Four factors made it seem profitable to reanalyse the Massonne & Szpurka data together with all other experimental data available. (1) Their activity model did not encompass the possibility of ordered site distributions as suggested in the recent studies of Pavese *et al.* (1997, 1999) and Smyth *et al.* (2000) in natural high-pressure phengite. A more ordered model predicts asymmetric mixing even when ideal, suggesting that a simple regular solution might suffice for dealing with non-ideality. (2) Given the large scatter in the experiments, the asymmetric Margules model used by Massonne & Szpurka appears unnecessary. (3) The molar volumes along the muscovite–celadonite solid solution have been recently measured (Schmidt *et al.*, 2001) and are different from those given in Massonne & Szpurka. (4) Thermodynamic data derived from the experiments of Massonne & Szpurka (1997) need to be made consistent with the garnet–phengite Fe/Mg exchange experiments of Green & Hellman (1982).

Although the experimental data are not reversals of composition at the desired run conditions (they are the results of synthesis runs), Massonne has made strenuous efforts to demonstrate that they show all the features expected of a close degree of attainment of equilibrium. For example, synthesis from different starting materials yielded the same mineral compositions, as did differing bulk compositions from within a given three-phase field under the same pressure and temperature conditions (Massonne & Schreyer 1986, 1987, 1989). In addition, the studies of Massonne & Szpurka (1997) and Holland & Powell (1998) showed that such experiments were amenable to a self-consistent thermodynamic treatment.

## DATA FITTING AND MODELS

One of the two goals of this study is to derive a set of thermodynamic data (enthalpy, entropy, volume, heat capacity, thermal expansion, compressibility) for the end-members of the mu–pa–cel–fcel white mica system. End-member data may be combined with thermodynamic data for other minerals to generate a number of new thermobarometers for use in high-pressure rocks. The second goal is to develop a mixing model for this solid solution to provide reliable activities for these end-members. The approach used is similar to that of Holland & Powell (1998) in which the enthalpies (and non-ideal mixing terms) are determined from experimental phase equilibrium data by the method of least squares.

### End-member data

All thermodynamic data for muscovite and paragonite are taken from Holland & Powell (1998).

The properties for celadonite and ferroceldonite will be estimated or determined as follows. Heat capacities and thermal expansivities are taken from Holland & Powell (1998), entropies are estimated from the algorithm in Holland (1989), and volume for celadonite taken from the recent study of Schmidt *et al.* (2001). Compressibilities are taken from Smyth *et al.* (2000). There is not enough information in Massonne & Szpurka (1997) to make a reliable estimation of molar volume for ferroceldonite, and so its volume is estimated by taking a number of Fe–Mg exchange reactions involving celadonite and ferroceldonite together with end-members in Fe–Mg solutions in the phases chloritoid, chlorite, biotite, olivine, orthopyroxene and clinopyroxene and assuming that the volume change for such exchange reactions is zero. Table 1 lists the basic thermodynamic data for the end-members. The enthalpies of formation of celadonite and ferroceldonite are derived from the phase equilibrium experiments, but as this requires knowledge of the mixing properties of the mu–cel and mu–fcel solid solutions, the mixing energies are derived simultaneously along with the enthalpies of formation of the end-members.

### Mixing properties of mica solid solutions in KFMASH

The ideal part of the Gibbs energy of mixing will be taken from the model outlined in Holland & Powell (1998) in which Mg and Al are assumed to order onto M2A and M2B sites such that each Mg tends to be surrounded by Al and vice versa, an assumption originally based on the strong tendency to order on the octahedral sites in omphacitic pyroxene. The ordering of Al and Si onto T1 and T2 type sites was originally suggested (Holland & Powell, 1990) to allow for Al avoidance and maximum dispersion of charges and because the entropy of muscovite and paragonite derived from phase equilibrium studies was far lower than that numerically predicted on the basis of tetrahedral disorder. There is recent supporting evidence for such ordering on octahedral and tetrahedral sites in phengite (Pavese *et al.*, 1997, 1999; Smyth *et al.*, 2000).

In determining the enthalpies of the end-members celadonite and ferroceldonite (and the mixing properties) the small vacancy substitution in the A site at the experimental pressures and temperatures is ignored. When calculated equilibrium site vacancies are taken into account, the curves in Figs 1, 2 and 4 are hardly changed (and are within the experimental uncertainties involved). The micas are assumed to be dioctahedral in this model and so the small trioctahedral content (a small excess over the assumption of two octahedral cations documented by Massonne & Schreyer, 1986) in the mica analyses will be ignored. This has a negligible thermodynamic effect on the results because (a) the activities of dioctahedral end-members are displaced very little from unity with such a small substitution

**Table 1.** Thermodynamic data refined in this study and those used in the calculated figures.  $H$  and  $sd(H)$  are enthalpy of formation and its standard deviation (kJ),  $S$  is the entropy (J/K),  $V$  is the molar volume (kJ/kbar),  $a_0$  is the thermal expansion parameter and  $\kappa$  is the bulk modulus.  $V_r$ ,  $S_r$ ,  $a_r$ ,  $\kappa_r$  are literature references for volume, entropy, thermal expansion and bulk modulus data. Heat capacities and Landau disorder terms are unchanged from Holland & Powell (1998). A complete revised data set for use with the program THERMOCALC is available from the website ([www.esc.cam.ac.uk/astaff/holland](http://www.esc.cam.ac.uk/astaff/holland)).

	$H$	$sd(H)$	$S$	$V$	$a_0$	$\kappa$	$V_r$	$S_r$	$a_r$	$\kappa_r$
phl	-6219.21	2.91	328.00	14.964	5.79	513	2	1,2	3	4
ann	-5151.86	3.12	418.00	15.432	5.79	513	5	1,2	0,3	0,4
east	-6338.21	3.05	318.00	14.738	5.79	513	6	31	0	0
mst	-25101.46	6.35	910.00	44.260	1.20	1200	7	0	0	8
fst	-23754.23	6.27	1010.00	44.880	1.20	1200	5	0	0	8
mctd	-3551.43	0.75	140.00	6.875	5.42	1465	9	31	10	11
fctd	-3215.46	0.78	155.00	6.980	5.42	1465	12	31	0	0
mcar	-4781.27	0.81	210.00	10.590	5.00	525	9	31	0	0
fcar	-4413.44	1.04	255.00	10.690	5.00	525	13	31	0	0
py	-6284.75	1.20	266.30	11.318	4.36	1737	2	2	14	15
alm	-5263.63	1.26	340.00	11.511	4.03	1690	17	2	14	16
afchl	-8727.50	2.32	428.00	21.660	3.98	870	18	31	0,18	0,19
clin	-8912.48	1.78	430.50	21.090	3.98	870	18	31	18	19
daph	-7135.35	2.56	565.00	21.340	3.98	870	7	31	0	0
ames	-9034.47	1.91	410.00	20.520	3.98	870	18	31	0,19	0,19
mu	-5984.18	2.91	292.00	14.083	5.96	490	2	1,2	20	21
cel	-5842.45	2.83	290.00	13.957	5.96	700	29	0	20	30
fccl	-5477.59	2.85	329.00	14.070	5.96	700	0	0	0,20	0,30
prl	-5640.62	1.11	239.40	12.810	7.50	525	2	2	22	0
ta	-5897.15	1.52	260.00	13.625	3.70	480	2	1,2	23	23
tats	-5987.76	1.15	259.00	13.510	3.70	480	0	0	0,23	0,23
fta	-4803.16	4.50	352.00	14.225	3.70	480	0	0	0,23	0,23
ky	-2593.11	0.67	83.50	4.414	4.04	1590	2	1,2	24	26
and	-2588.75	0.67	92.70	5.153	4.11	1334	2	1,2	24	25
sill	-2585.86	0.67	95.50	4.986	2.21	1320	2	1,2	24	26
q	-910.84	0.34	41.50	2.269	0.650	750	2	2	27	27
coe	-905.49	0.34	40.80	2.064	1.80	1000	2	1,2	14	28
H <sub>2</sub> O	-241.81	0.02	188.80	0	0	0		2		

References for  $V$ ,  $S$ ,  $a_0$  and  $\kappa$ :

0 Estimated; 1 Adjusted in Holland & Powell (1998); 2 Robie & Hemingway (1995); 3 Takeda & Morosin (1975); 4 Hazen & Finger (1978); 5 Robie *et al.* (1967); 6 Hewitt & Wones (1975); 7 Schreyer & Seifert (1969); 8 Birch (1966); 9 Chopin & Schreyer (1983); 10 Ivaldi *et al.* (1988); 11 Comodi *et al.* (1991); 12 Rao & Johannes (1979); 13 Viswanathan & Seidel (1979); 14 Skinner (1966); 15 Hazen *et al.* (1994); 16 Sato *et al.* (1978); 17 Chatillon-Colinet *et al.* (1983); 18 Nelson & Guggenheim (1993); 19 Hazen & Finger (1978); 20 Guggenheim *et al.* (1987); 21 Comodi & Zanazzi (1994); 22 Symmes (unpublished data 1986) quoted in Berman (1988); 23 Pawley *et al.* (1995); 24 Winter & Ghose (1979); 25 Ralph *et al.* (1984); 26 Brace *et al.* (1969); 27 Dorogokupets (1995); 28 Levien & Prewitt (1981); 29 Schmidt *et al.* (2001); 30 Smyth *et al.* (2000); 31 Adjusted in this study. Additionally, entropies of all chlorite end-members have been incremented by 20 J K<sup>-1</sup> relative to Holland & Powell, 1998).

(b) the solvus between dioctahedral and trioctahedral micas implies positive activity coefficients which would offset any such reduction in activity, and (c) muscovite and celadonite occur on opposite sides of the reactions used (see below) such that any effect is largely self-cancelling.

The site partitioning scheme used is shown in Table 2 and the ideal activities are then given by

$$a_{\text{mu}}^{\text{ideal}} = 4X_{\text{K}}^A X_{\text{Al}}^{M2A} X_{\text{Al}}^{T1} X_{\text{Si}}^{T1} = (1-z)y^2(2-y)$$

$$a_{\text{cel}}^{\text{ideal}} = X_{\text{K}}^A X_{\text{Mg}}^{M2A} (X_{\text{Si}}^{T1})^2 = \frac{1}{4}(1-z)(1-y)(1-x)(2-y)^2$$

$$a_{\text{fccl}}^{\text{ideal}} = X_{\text{K}}^A X_{\text{Fe}}^{M2A} (X_{\text{Si}}^{T1})^2 = \frac{1}{4}(1-z)(1-y)x(2-y)^2$$

$$a_{\text{pa}}^{\text{ideal}} = 4X_{\text{Na}}^A X_{\text{Al}}^{M2A} X_{\text{Al}}^{T1} X_{\text{Si}}^{T1} = zy^2(2-y)$$

where the  $x$ ,  $y$  and  $z$  variables are defined as

$$y = X_{\text{Al}}^{M2A}$$

$$x = \left( \frac{\text{Fe}}{\text{Fe} + \text{Mg}} \right)^{\text{mica}}$$

$$z = X_{\text{Na}}^A$$

In the simple KFASH and KMASH systems,  $x = 1$  and  $x = 0$ , respectively, and  $z = 0$ .

**Table 2.** Site partitioning scheme used.

	A	M2A	M2B	T1	T2
Mu	K	Al	Al	Al Si	Si <sub>2</sub>
Cel	K	Mg	Al	Si Si	Si <sub>2</sub>
Fcel	K	Fe	Al	Si Si	Si <sub>2</sub>
Pa	Na	Al	Al	Al Si	Si <sub>2</sub>

Non-ideal contributions to the activity are initially assumed to be symmetrical, and so a regular solution among the four end-members is used. The regular solution is taken macroscopically and uses the proportions of the end-members ( $p_{\text{pa}} = z$ ,  $p_{\text{cel}} = (1-x)(1-y)$ ,  $p_{\text{fccl}} = x(1-y)$ ,  $p_{\text{mu}} = y-z$ ) in the expressions for excess Gibbs energy of mixing and activity coefficient

$$G_{\text{ex}} = \sum_i \sum_{j>i} p_i p_j W_{ij}$$

$$RT \ln \gamma_q = - \sum_i \sum_{j>i} y_i y_j W_{ij}$$

$$y_k = \delta - p_k. \quad \delta = 1 \text{ when } k = q \text{ otherwise } \delta = 0$$

Here  $G_{\text{ex}}$  is the excess Gibbs energy of mixing,  $\gamma_q$  is the activity coefficient of end-member  $q$  and the  $W_{ij}$  are the

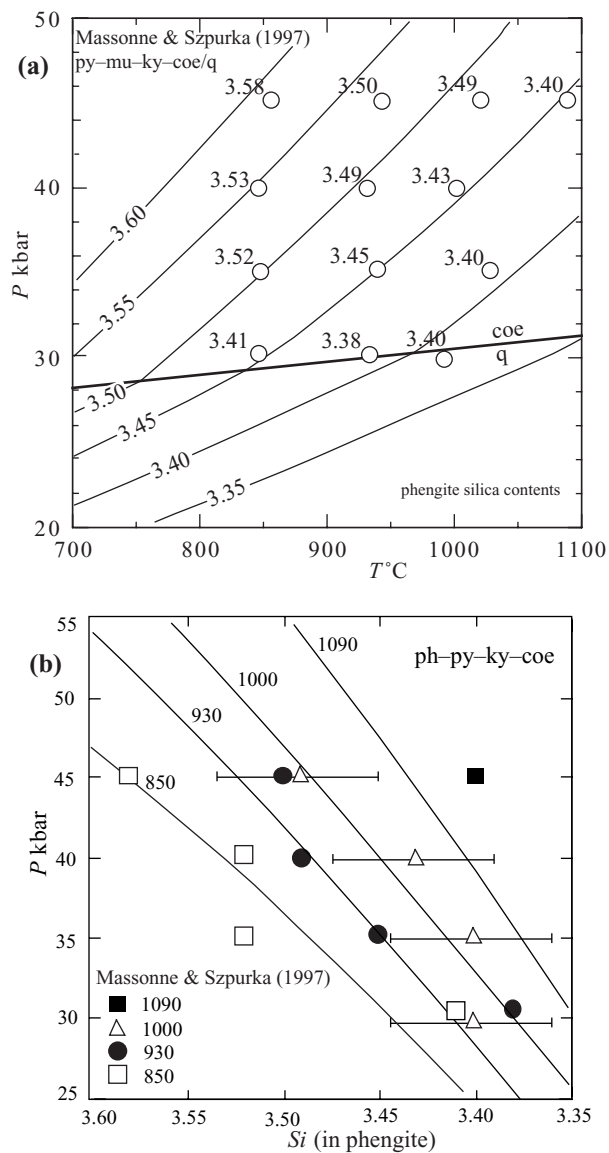


**Fig. 1.** Experimental results and calculated curves for silica content of phengite coexisting with pyrope, kyanite and quartz/coesite in KMAH. (a)  $P$ ,  $T$  diagram showing calculated isopleths and experimental compositions reported by Massonne & Szpurka (1997). (b) Isotherms on a pressure-composition diagram which shows the experimental scatter more clearly. Error bars from the original authors' estimates are shown for only one isotherm to retain clarity in the figure.

interaction energies for an  $ij$  pair in the regular solution model. Note that there is no requirement for all the end-member proportions to be positive — it is sufficient that they form an independent set which sums to unity. In the course of this study several other mixing model assumptions were investigated. The earlier disordered model (e.g. Holland & Powell, 1990) did not fit the data so well, and a molecular-type model is difficult to apply unambiguously in multicomponent systems. A third model, involving ordering within the T1 sites, also

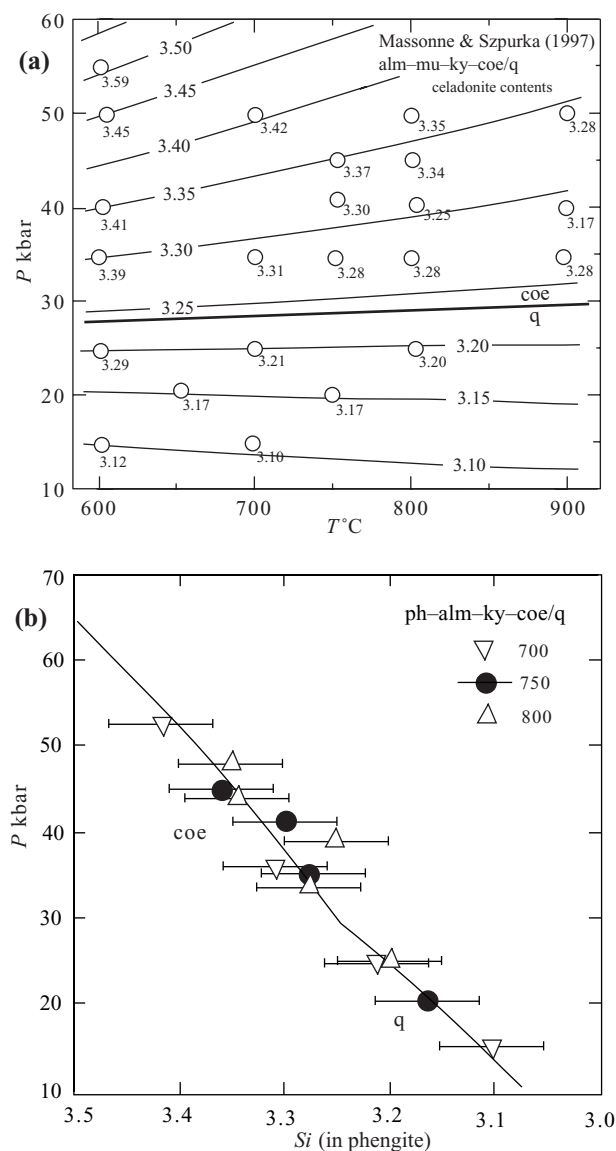


**Fig. 2.** Experimental results and calculated curves for silica content of phengite coexisting with almandine, kyanite and quartz/coesite in KFAH. (a)  $P$ ,  $T$  diagram showing calculated isopleths and experimental compositions reported by Massonne & Szpurka (1997). (b) Pressure-composition diagram at 750 °C showing experimental data from the range 700–800 °C. Data points at 700 and 800 °C are corrected to an apparent 750 °C pressure by moving them parallel to the isopleths in (a). The calculated curve is in excellent agreement with the measured data. Error bars are from the original authors' estimates. The degree of scatter in the experimental study below 700 °C and above 800 °C is considerable and is not shown.

performed significantly worse than the model chosen above.

#### Phase equilibrium constraints in Na-free systems

There are five assemblages in which phengite compositional data have been experimentally deter-

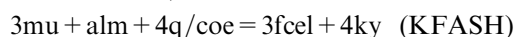
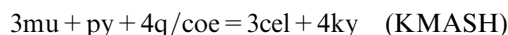
mined: (1) garnet + phengite + kyanite + quartz/coesite in KMASH + KFLASH (Massonne & Szpurka, 1997); (2) talc + phengite + kyanite + quartz/coesite in KMASH (Massonne & Schreyer, 1989); (3) phlogopite + phengite + k-feldspar + quartz in KMASH (Massonne & Schreyer, 1987); (4) talc + phengite + phlogopite + kyanite + quartz/coesite in KMASH (Massonne & Schreyer, 1989); and (5) garnet + phengite in KFMASH Fe–Mg exchange experiments (Green & Hellman, 1982).

Assemblages (3) and (4) are less useful in that they involve phlogopite, whose alumina content varies and is not well determined at the pressures and temperatures of the experiments. Although experiments for assemblage (5) were performed with natural minerals, the amounts of other elements such as Na, Ca, Mn were vanishingly small and the system approximates closely enough to KFMASH that the effects of these impurities may be safely ignored. Although the alumina contents of talc are too small to introduce significant error, they are accounted for using the thermodynamic data for talc and aluminous talc derived by Holland & Powell (1998) from the experimental results of Hoschek (1995).

## METHODS OF ANALYSIS

The mineral end-member abbreviations used here are shown in Table 3.

Garnet + phengite + kyanite + quartz/coesite assemblages provided by Massonne & Szpurka (1997) buffer the composition of the phengite according to the equilibrium:



for which the equilibrium condition in KMASH may be stated as

$$0 = \Delta G_{1\text{bar},T}^{\circ} + \int_{1\text{bar}}^P \Delta V dP + 3RT \ln \frac{a_{\text{cel}}}{a_{\text{mu}}}$$

with a similar statement involving fcel in place of cel for KFLASH. In the above expression  $\Delta G_{1\text{bar},T}^{\circ}$  is the standard Gibbs energy of reaction for the pure end-members at 1 bar pressure and arbitrary temperature, and  $\Delta V$  is the volume change for the end-members at  $P$  and  $T$ .

**Table 3.** Mineral end-member abbreviations used.

Phengite (ph):	mu	muscovite	$\text{KAl}_2(\text{AlSi}_3)\text{O}_{10}(\text{OH})_2$
	cel	celadonite	$\text{KMgAl}(\text{Si}_4)\text{O}_{10}(\text{OH})_2$
	fcel	ferroceladonite	$\text{KFeAl}(\text{Si}_4)\text{O}_{10}(\text{OH})_2$
garnet:	py	pyrope	$\text{Mg}_3\text{Al}_2\text{Si}_3\text{O}_{12}$
	alm	almandine	$\text{Fe}_3\text{Al}_2\text{Si}_3\text{O}_{12}$
talc	ta		
kyanite	ky		
quartz	q		
coesite	coe		

The activities of celadonite and muscovite are model-dependent, and the model of Holland & Powell (1998) as discussed above is used. This simple activity model yields a Gibbs free energy of mixing which has the same sense of asymmetry as suggested by Massonne & Szpurka's more complex asymmetric Margules model. In principle, the experimentally determined values for phengite composition at various pressures and temperatures may be used to determine values for enthalpy, entropy, volume and interaction energy ( $W_{\text{mu-fcel}}$ ) by regression. However, in practice, the terms may be highly correlated, and the experimental range in  $P$  or  $T$  may not be large enough to determine the volume or entropy accurately. Thus, as a start, the volumes will be assumed known and taken from the study of Schmidt *et al.* (2001), and entropies taken as estimated above. The experiments were used to determine initial values for  $W_{\text{mu-cel}}$ ,  $W_{\text{mu-fcel}}$  and the enthalpies of formation of cel and fcel by regression.

## Fitting all the available equilibria simultaneously

Although a set of consistent thermodynamic data for KMASH and KFLASH may be retrieved from the two experimental studies above, such a set needs also to be capable of reproducing the experimental phase equilibria which have been published for the assemblage talc + phengite + kyanite + quartz (or coesite) in KMASH and the garnet–phengite Fe–Mg exchange experiments in the larger KFMASH system.

Inclusion of these assemblages allows writing of the following six equilibria which may be applied to the experimental data to refine further the values of the thermodynamic properties of celadonite and ferroceladonite and the interaction energy. The six reactions, listed under each assemblage, are as follows

1.  $3\text{cel} + 4\text{ky} = \text{py} + 3\text{mu} + 4\text{coe}$
2.  $3\text{fcel} + 4\text{ky} = \text{alm} + 3\text{mu} + 4\text{coe}$
3.  $3\text{fcel} + 4\text{ky} = \text{alm} + 3\text{mu} + 4\text{q}$
4.  $3\text{cel} + 3\text{ky} + \text{H}_2\text{O} = \text{ta} + 3\text{mu} + \text{q}$
5.  $3\text{cel} + 3\text{ky} + \text{H}_2\text{O} = \text{ta} + 3\text{mu} + 2\text{coe}$
6.  $3\text{fcel} + \text{py} = \text{alm} + 3\text{cel}$

These six reactions will be used to determine the enthalpies of formation of celadonite and ferroceladonite as well as the regular solution energies for muscovite–celadonite and muscovite–ferroceladonite. If the compositions of all phases are known at each  $P$ ,  $T$  experiment, then six equilibrium equations of the form  $0 = \Delta G_{PT}^{\circ} + RT \ln K$  may be written and the system solved for the desired parameters by the method of least squares. All terms which make up the Gibbs energy of the end-member reaction ( $\Delta G_{PT}^{\circ}$ ) are calculated using the thermodynamic data of Holland & Powell (1998), all constituent ideal activities in the

$RT \ln K$  term are made up from the activity model for phengite above together with the ideal mixing model for talc from Holland & Powell (1998). Thus the unknowns are the heats of formation of celadonite and ferroceldonite and values for  $W_{\text{mu-cel}}$  and  $W_{\text{mu-fcel}}$ . The measured molar volumes (Schmidt *et al.*, 2001) indicate that there is an approximately symmetrical excess volume of mixing, which implies that the  $W_{\text{mu-cel}}$  parameter is pressure-dependent.  $W_{\text{mu-cel}}$  is taken to be linear in pressure  $W_{\text{mu-cel}} = a + bP$ , with  $b$  taken as  $0.2 \text{ kJ kbar}^{-2}$  from Schmidt *et al.* (2001). We have assumed that the muscovite–ferroceldonite solid solution shows an identical pressure coefficient.

A computer program was written to read in a file of these reactions, pressures, temperatures and mineral compositions, to set up the equilibrium relation for each reaction at the relevant pressure and temperature for each experiment, and to perform the least squares regression. The input mineral compositions are simply the Si content of the phengite for reactions (1)–(5), the calculated compositions for talc in reactions (4)–(5), and the Fe/(Fe + Mg) ratios of phengite and garnet for reaction 6. Because the garnet in the experiments for reaction  $3\text{fcel} + \text{py} = \text{alm} + 3\text{cel}$  is an almost pure almandine–pyrope solid solution, the non-ideality in garnet has been taken from a simple binary regular solution model with  $W_{\text{py-alm}} = 2.5 \text{ kJ}$  (Holland & Powell, 1998). The results of regression of all the experiments using the six equilibria above are given as thermodynamic data in Table 1. The two  $W$  terms were within error of zero at the 2 standard deviation level and so were set at zero for a final optimisation stage to refine the enthalpies of celadonite and ferroceldonite.

After optimising the enthalpies of celadonite and ferroceldonite as above, the six reactions were used in the input file for the program LSQDS to update the thermodynamic data set as documented in Holland & Powell (1998). This step is necessary in order to derive the uncertainties and correlations for the enthalpies, and results in a data set in which the enthalpies of all end-members other than celadonite and ferroceldonite are essentially unchanged. With this improved data set, new thermobarometers may be applied to natural high-pressure phengite-bearing rocks to determine better their conditions of formation.

## RESULTS AND DISCUSSION

The three key sets of equilibria in determining the properties of celadonite and ferroceldonite are the first three reactions listed above for the assemblage garnet + phengite + kyanite + quartz/coesite. Calculated isopleths for phengite Si content and experimental points are shown in Fig. 1(a) for the KMASH system. The degree of scatter in the original experiments is considerable and is not particularly obvious in Fig. 1(a), but shows up clearly on the  $P$ – $Si$  plot in Fig. 1(b). The scatter is probably an unavoidable result of the difficulty of working with syntheses from reactive starting material.

The analogous data for the KFASH data are shown in Fig. 2(a,b). The experimental data in the range 650–800 °C, although somewhat scattered, show a fairly good trend in Fig. 2(b). The curve in Fig. 2(b) was drawn for a temperature of 750 °C and the data points have been moved along the isopleths of Fig. 2(a) to give the apparent pressures at this temperature for comparison. Apart from one datum at 800 °C the experiments cluster nicely about the calculated curve. The data at 600 and 900 °C are very scattered and were not used in the regression. It is likely that the lowest temperature experiments suffered from incomplete equilibration. The reason for the scatter in the highest temperature data is uncertain, but one possibility is that they may have involved a small degree of partial melting, with disequilibrium mica growing rapidly on quench.

The Fe–Mg exchange experiments of Green & Hellman (1982) make a useful tie between the KMASH and KFASH experiments of Massonne & Szpurka (1997) and provide a test of mutual agreement among the experimental studies. Of the available garnet–phengite experimental exchange data those of Green & Hellman (1982) are extremely close to the FMASH system, and hence require no additional factors to consider. The experimental values of  $\ln K$  (reduced to 1 bar values) are shown in Fig. 3 along with the best fit curve calculated with thermodynamic data from this study. Three natural garnet–phengite pairs from the study of Hynes & Forest (1988) have been included to illustrate the good agreement of the low temperature extrapolation of the derived thermodynamic data. It would be difficult to define a reliable thermometer from the Green & Hellman experimental data alone, and the constraints from the KMASH and KFASH systems of Massonne & Szpurka (1997) help determine the slope to fit through the data in Fig. 3. The three studies taken together provide very tight constraints on the thermodynamic data for celadonite and ferroceldonite. The mixing energetics were within error of  $W_{\text{cel-fcel}} = 0.0$  and so the Fe–Mg mixing is taken as ideal.

The experiments of Massonne & Schreyer (1989) on phengite compositions coexisting with talc and kyanite are also useful, but less constraining, in fitting the mica thermodynamics. The degree of scatter in the original experiments is larger than for the experiments of Massonne & Szpurka (1997), as can be seen in Fig. 4(a,b). Nevertheless, the trend in Fig. 4(b) is in very good agreement with the measured volume and the estimated entropy of celadonite. The calculated alumina contents of talc in these experiments lie in the range  $X_{\text{Al,M1}} = 0.02$ – $0.07$ , and so the activity of talc remains close to unit value.

The three fluid-absent reactions studied here and the eclogite barometer of Waters & Martin (1993) may make useful thermobarometers for eclogites and other high-pressure assemblages, and the thermodynamics in linearised form are given in Table 4 as

$$0 = a + bT + cP + RT \ln K \text{ (units of kJ, kbar, K).}$$

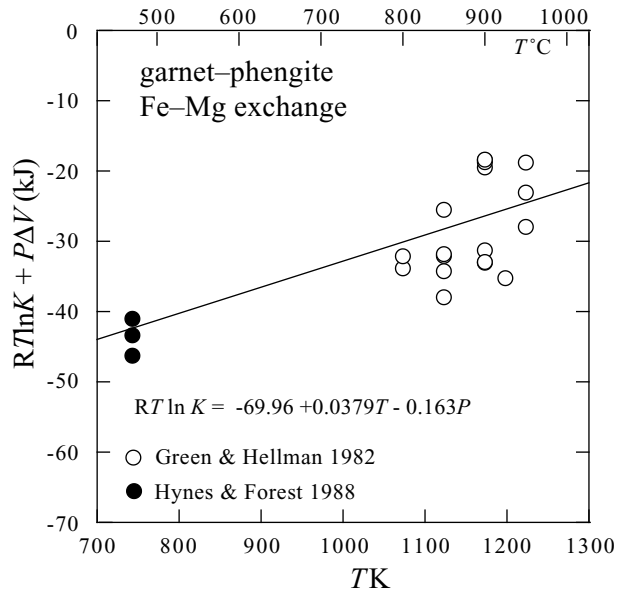


**Fig. 3.** Plot of  $RT \ln K + P\Delta V$  against  $T$  for the garnet–phengite Fe–Mg exchange experiments of Green & Hellman (1982) and natural pairs from Hynes & Forest (1988). The calculated curve is also constrained by fits to experiments in KMASH (Fig. 1) and KFLASH (Fig. 2) and is in acceptable agreement with the experimental values (which on their own would not yield an unambiguous slope). The extrapolation to low temperatures is seen to be in good agreement with the study of Hynes & Forest (1988).

Because it is difficult to determine accurately the activity of ferrocaldonite in Mg-rich phengite due to the inherent uncertainty in assigning an appropriate amount of  $\text{Fe}^{3+}$  from a microprobe analysis, the thermometers and barometers involving fcel should be used with caution, particularly for Fe-poor phengite.

#### Micas in the NKFMASH system

For phase diagram calculations in model systems approaching the complexity of natural rocks, and for activity models for use in thermobarometry, it is necessary to include at least the addition of Na to the simple KFMASH micas considered so far. The obvious end-member to include is paragonite ( $\text{NaAl}_2[\text{AlSi}_3]\text{O}_{10}(\text{OH})_2$ ), whose thermodynamic properties are already well constrained through direct measurement and fitting to numerous phase equilibrium experiments. However, the mixing properties between paragonite and the other end-members require determination.

Natural paragonite–muscovite pairs are related by a solvus, and Rosenfeld *et al.* (1958) suggested that the compositions of coexisting paragonite–muscovite pairs could be used to measure the final equilibration temperatures of metamorphic assemblages. Attempts have been made to determine the solvus limbs experimentally through phase equilibrium, calorimetry or by cation exchange (Eugster *et al.*, 1972; Pascal & Roux, 1985;

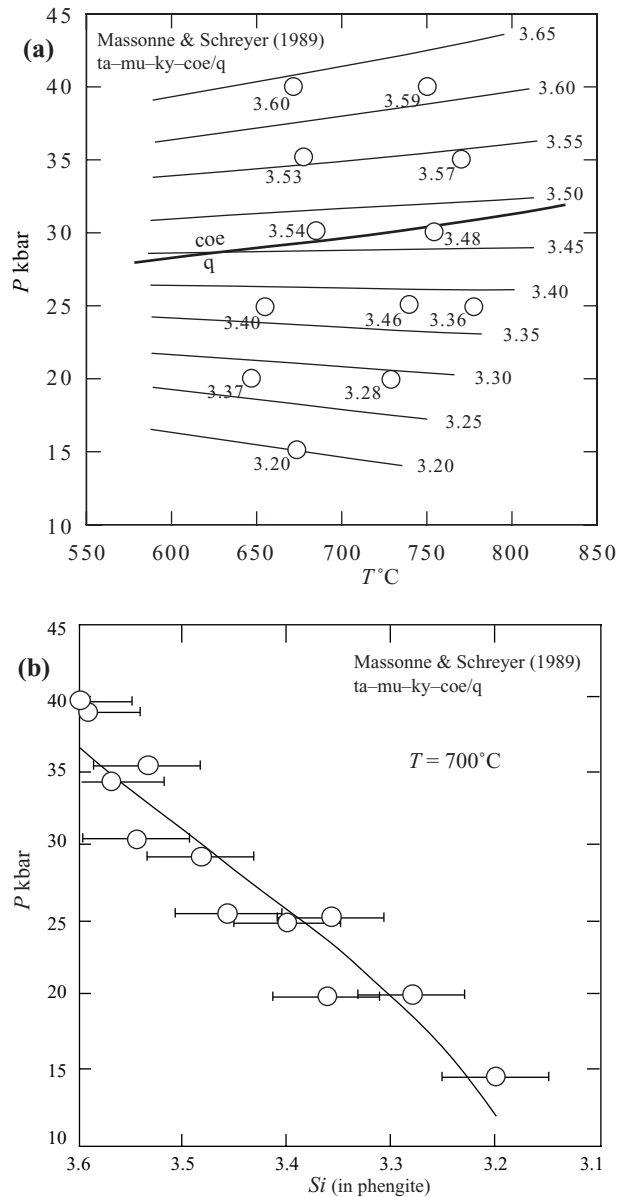


**Fig. 4.** Experimental results and calculated curves for silica content of phengite coexisting with talc, kyanite and quartz/coesite in KMASH. (a)  $P$ ,  $T$  diagram showing experimental compositions reported by Massonne & Schreyer (1989) and calculated isopleths. (b) Pressure–composition diagram at  $700^\circ\text{C}$  showing experimental data from (a). Data points are corrected to apparent pressures at  $700^\circ\text{C}$  in (a) by moving them parallel to the isopleths. The calculated slope and position are in good agreement with the measured data, given the degree of scatter in the experimental study. Error bars are from the original authors' estimates.

Chatterjee & Flux, 1986; Flux & Chatterjee, 1986; Roux & Hovis, 1996). Guidotti *et al.* (1994), in a study of natural solvus pairs, noted that the two main controls on the width of the solvus were pressure and the silica content in the potassic mica, both of which lead to widening of the solvus gap. Separating these two effects

**Table 4.** Thermodynamics in linearised form for the three fluid-absent reactions and the eclogite barometer.

	a	sd(a)	b	c
py + 3fcel = alm + 3cel	-70.36	1.18	0.03823	-0.158
py + 3mu + 4q = 3cel + 4ky	-23.23	0.93	0.10038	-2.552
alm + 3mu + 4q = 3fcel + 4ky	47.13	0.91	0.06215	-2.393
py + 2gr + 3cel = 6di + 3mu	-62.57	1.85	-0.08625	3.164

from natural occurrences is not easy without thermodynamic models, because the increase in silica content in phengite depends in large part on the pressure of metamorphism. Roux & Hovis (1996) performed additional calorimetry on the muscovite–paragonite system, reviewed the available data and derived a new thermodynamic model for the NKASH system.

The Roux and Hovis analysis of the available data is accepted here, but is recast from their subregular Margules model into a van Laar formalism because it is more convenient to use in multicomponent solutions. In the van Laar model, mixing energetics for a binary are accommodated via a single interaction energy  $W$  (as in the regular solution) and asymmetry is introduced by assigning a pseudovolume to each end-member in the solution. The binary activity coefficients in such a van Laar formalism are given by

$$RT \ln \gamma_1 = \frac{2V_1}{V_1 + V_2} W_{12} \Phi_2^2$$

$$RT \ln \gamma_2 = \frac{2V_2}{V_1 + V_2} W_{12} \Phi_1^2$$

where

$$\Phi_1 = \frac{X_1 V_1}{(X_1 V_1 + X_2 V_2)} \quad \text{and} \quad \Phi_2 = \frac{X_2 V_2}{(X_1 V_1 + X_2 V_2)}.$$

$V_1$  and  $V_2$  are the effective volumes of end-members 1 and 2 and differ from the real volumes in representing the effective volume mismatch or strain for the mixing entities.  $\Phi_1$  and  $\Phi_2$  are volume proportions of the end-members in the solution. When  $V_1 = V_2$  the volume proportions become mole fractions and the model reduces to a regular solution. It is only the relative magnitudes of  $V_1$  and  $V_2$  which matter, and here they are scaled to sum to unity. The preferred solvus of Roux and Hovis can be reproduced using the following van Laar model parameters

$$W_{\text{mu-pa}} = 10.12 + 0.0034T + 0.353P \text{ (units kJ, kbar, K)}$$

$$V_{\text{mu}} = 0.63$$

$$V_{\text{pa}} = 0.37$$

In the four end-member system muscovite–paragonite–celadonite–ferroceladonite, only two of the six interaction energies ( $W_{\text{pa-fcel}}$  and  $W_{\text{pa-cel}}$ ) remain to be determined. The values for the other four were determined above and may be summarised as

$$W_{\text{mu-pa}} = 10.12 + 0.0034T + 0.353P$$

$$W_{\text{mu-cel}} = 0.2P$$

$$W_{\text{mu-fcel}} = 0.2P$$

$$W_{\text{cel-fcel}} = 0.0$$

The extension of the van Laar model to multicomponent solutions is straightforward and is discussed in a forthcoming paper (Holland & Powell, in prep.). All potassic end-members (mu, cel, fcel) are assumed to have the same pseudovolume (0.67) because of the apparent symmetry in the measured volumes along the mu–cel join. Also, because of the ideal Fe–Mg mixing it is likely that  $W_{\text{pa-fcel}}$  and  $W_{\text{pa-cel}}$  are identical, so that only one parameter needs to be found to complete the model. The natural solvus data in Guidotti *et al.* (1994) and in particular the compositions of coexisting paragonite and phengite from the Tauern Window (assumed to be 20 kbar, 600 °C) may be used to calibrate the remaining non-ideal terms. A value for  $W_{\text{pa-fcel}} = W_{\text{pa-cel}} = 52$  kJ allows the solvus to widen enough to agree with the Tauern micas, and the calculated solvus limbs are shown as functions of pressure and celadonite content in Fig. 5. The diagrams in Fig. 5 are calculated using THERMOCALC v3.1 which can accept the van Laar model, and is now available on the Web. The NKASH solvus (at Si = 3.0) is a strong function of pressure (Fig. 5a), but also extremely sensitive to small increases in celadonite content in the phengite limb (Fig. 5b), where the effect of 10% celadonite (Si = 3.1) is greater than a pressure increase of 5 kbar (compare Fig. 5a,b). Thus small increases in silica content of phengite over that in the NKASH system have sufficiently large effects that use of two-mica solvus thermometry may be of limited practical application. As noted by Roux & Hovis (1996), there is considerable uncertainty in determining the position of the limbs even for the simple NKASH solvus, as can be seen from the two conflicting sets of experimental brackets shown in Fig. 5. The earlier experimental solvus determination by Eugster *et al.* (1972) calls for a wider more symmetric solvus, while that based on cation exchange studies (Flux & Chatterjee, 1986) is both narrower and more asymmetric. The natural data collated by Guidotti *et al.* (1994) lie mostly in between, and inspection of Fig. 5(b) suggests that this might be expected where increased celadonitic substitutions tend to progressively widen a relatively narrow NKASH solvus. Nevertheless, given the uncertainties in the experimental data, the results suggested here must be considered provisional.

## APPLICATIONS

Two brief applications will be made here. The first involves thermobarometry of the famous pyrope–coesite rock (sample 2–39 of Chopin, 1984) from Parigi in the Dora Maira massif, western Alps (Chopin, 1984; Schertl *et al.*, 1991). The rock has an extremely high

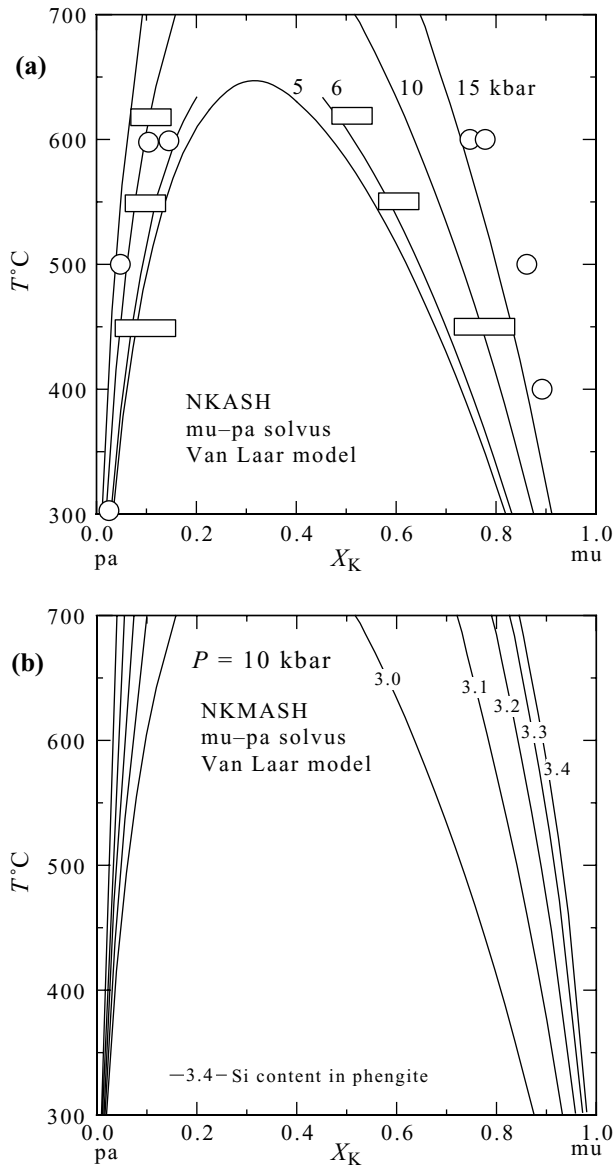


**Fig. 5.** Calculated muscovite–paragonite solvi. (a) The effect of pressure on the solvus, using the van Laar mixing model calibrated on the data of Roux & Hovis (1996). Boxes are experimental data of Flux & Chatterjee (1986) at 5, 6 and 7 kbar, and circles are experimental data of Eugster *et al.* (1972) at 2 kbar. (b) The effect of increasing the silica content of the phengite (in NKMASH) at a fixed pressure of 10 kbar.

Mg/(Fe + Mg) ratio and contains pyrope, phengite, kyanite, talc and coesite. Although the rock is very close to KMASH in composition and its pressures could be crudely read from the isopleths of silica content in Figs 1 and 4, a proper thermobarometric and phase diagram approach leads to improved estimates of metamorphic conditions. The program THERMOCALC was used to generate a phase diagram for a magnesian aluminous quartzite with excess coesite and H<sub>2</sub>O (the bulk composition was approximated from the natural phase compositions of pyrope, talc,

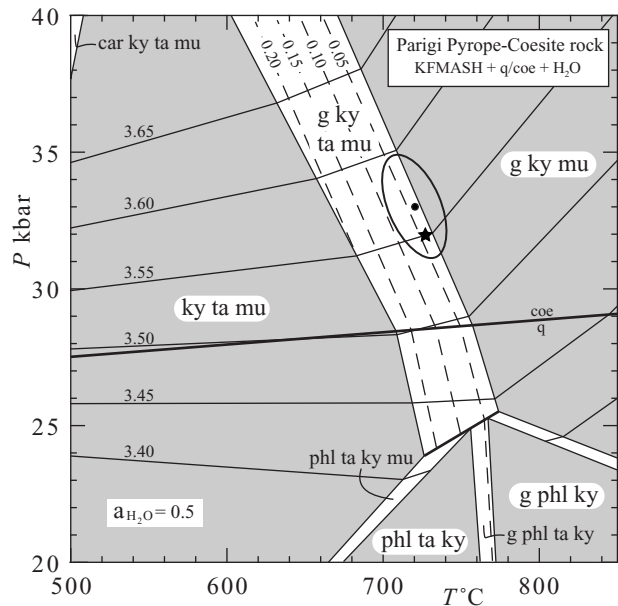


**Fig. 6.** *P*, *T* pseudosection and thermobarometry results for the pyrope–coesite rock 2–39 of Chopin (1984), calculated for a fixed water activity of 0.5. The diagram is contoured for silica content of phengite (continuous thin lines) and Fe/(Fe + Mg) ratio of garnet (dashed lines). The calculated conditions for rock 2–39 are indicated by the black star (model KFMASH prediction) and black dot with error ellipse (average *PT* thermobarometry using rock 2–39 mineral compositions). g = garnet, car = carpholite, ta = talc, ky = kyanite, phl = phlogopite, mu = muscovite (phengitic), coe = coesite, q = quartz.

phengite and kyanite in the proportions 2:1:2:1 giving the molar bulk composition as Al<sub>2</sub>O<sub>3</sub> = 41, MgO = 51, FeO = 1, K<sub>2</sub>O = 7). The first attempt to draw a diagram showed the same topology as in Fig. 6, but with the garnet–kyanite–talc field at temperatures some 60 °C higher than shown. Temperatures closer to 725–740 °C, based on stable isotope thermometry, are believed to be more appropriate for these rocks (C. Chopin, personal communication, 2002). Lowering the water activity to 0.5 has the effect of reducing the calculated temperatures by the required amount, and the suggestion that these rocks may once have been part of a meta-evaporite sequence might suggest that a saline brine could have been responsible for the reduction in water activity. Figure 6 has been constructed for a water activity of 0.5, and shows that the Parigi assemblage has a restricted temperature range (centred on 650 °C at 40 kbar to 750 °C at 28 kbar), losing garnet at lower temperatures and losing talc at higher temperatures. The conditions of formation may be deduced more precisely by considering the isopleths of Fe/(Fe + Mg) in pyrope (the dashed lines in Fig. 6) and the silica content of the phengite (thin continuous isopleths). The rock 2–39 has pyrope with Fe/(Fe + Mg) = 0.97 and a phengite with Si = 3.55 and therefore is predicted to have formed at 32 kbar and 730 °C (the black star in Fig. 6). At these

conditions the assemblage is predicted to contain 30% pyrope + 40% phengite + 15% talc + 15% kyanite with excess coesite. A small (< 2%) proportion of pyrophyllite substitution is predicted (see discussion of the next example) to occur in the micas at these conditions. At 32 kbar and 730 °C a halite-saturated fluid is calculated to contain 38% NaCl and 62% H<sub>2</sub>O, which corresponds to a water activity of 0.49, thus lending support to the suggestion of a strong brine as the agent for lowering water activity. The thermodynamic data for liquid NaCl and the activity model for the NaCl–H<sub>2</sub>O solution are derived from the experimental study of Aranovich & Newton (1996). In particular, the activities are given by:

$$a_{\text{NaCl}} = \frac{4(1-x)^2}{(2-x)^2} \exp\left(\frac{W}{RT}x^2\right)$$

$$a_{\text{H}_2\text{O}} = \frac{h}{(2-x)} \exp\left(\frac{W}{RT}(1-x)^2\right)$$

where  $x$  is the mol fraction of H<sub>2</sub>O and  $W$  (= 4.0 kJ) is a regular solution interaction energy for the NaCl–H<sub>2</sub>O binary.

The small black dot and associated error ellipse on Fig. 6 (at the one standard deviation level) come from using a multireaction approach to thermobarometry (the average  $PT$  method of Powell & Holland, 1994) on rock 2–39, also setting water activity at 0.5. The details of the calculation are given in Table 5. The average  $PT$  is close, but not identical, to the phase diagram estimate of physical conditions. Both methods are associated with their own sources of uncertainty. The phase diagram approach uses the model system KFMASH (and hence ignores the effects of small amounts of minor components such as Na<sub>2</sub>O, CaO, MnO, Fe<sub>2</sub>O<sub>3</sub>) whereas the average  $PT$  method, although allowing for the additional components, suffers from the fact that the activity model for such a natural multicomponent solution is poorly defined and from some microprobe errors, particularly in determination of ferric iron. The two approaches give remarkably similar  $PT$  estimates, perhaps not surprisingly, given that the natural rock is so close to KMASH in composition.

The second practical application is to take a typical average Dalradian pelite bulk composition (from Atherton & Brotherton, 1982) and calculate the pressures at which biotite disappears from pelitic assemblages to produce garnet–phengite schists. The bulk composition has been projected from plagioclase into the KFMASH subsystem. Thus Na and Ca are removed, along with the amount of Al and Si in the albite and anorthite, respectively. The bulk composition in molar proportions is Al<sub>2</sub>O<sub>3</sub> = 43.40, MgO = 19.50, FeO = 23.60, K<sub>2</sub>O = 13.50, and silica is taken in excess (quartz saturation assumed). The procedures for calculating pseudosections for pelitic bulk compositions are given in Powell *et al.* (1998), and the calculated diagram for average Dalradian pelite is shown in Fig. 7.

In generating this diagram the entropies of Mg-chloritoid and Fe-chloritoid have been updated (Table 1) so that the thermodynamic data set reproduces the important and careful study of Fe–Mg partitioning between chlorite and chloritoid by Vidal *et al.* (1999) at temperatures down to 300 °C. Such natural assemblage studies are extremely valuable in helping constrain models which are otherwise only fitted to relatively high-temperature experiments. The properties of the eastonite end-member of biotite were also modified slightly from those in Holland & Powell (1998), to allow agreement between calculated and natural alumina compositions of biotite in regional metamorphic pelites, such as those from the Al<sub>2</sub>SiO<sub>5</sub> triple point at Mt Moosilauke (Hodges & Spear, 1982). This was accomplished by raising the entropy of eastonite slightly and deriving its enthalpy from the same constraints used in Holland & Powell (1998).

Of major interest, because of the role of silica content in phengite, is the disappearance of biotite in typical pelite bulk compositions, and its replacement by phengitic muscovite. Above around 630 °C the assemblages lose biotite at around 13 kbar, leading to simple garnet–phengite and garnet–phengite–kyanite schists and are typical of assemblages seen in such leucocratic pelitic schists of high-pressure terranes such as the Tauern window, Austria, the Adula Nappe, Switzerland (Heinrich, 1982) or other high grade parts of the western Alps (Chopin, 1981).

The possibility, in terms of an AFM diagram, of a garnet–phengite–kyanite schist for typical pelite compositions is a peculiarity of the projection itself. As the celadonite content of the muscovite rises, the projected composition of both biotite and the rock bulk composition move steadily towards the A apex of the AFM projection, allowing typical bulk compositions to plot at apparently more aluminous locations than garnet. Figure 7 is contoured with isopleths of silica content in phengite showing the dominance of the role of pressure over that of temperature for almost all assemblages, and the barometric potential for phengite content in typical pelitic assemblages. The assemblage carpholite + chlorite gives way to carpholite + chloritoid + chlorite and chloritoid + chlorite assemblages in the region of 370–420 °C at 15–17 kbar (Fig. 7) in good agreement with the thermobarometric study of such a progression from the Western Alps by Agard *et al.* (2001). The ubiquitous retrogression to chlorite observed by Agard *et al.* is also readily explained by decompression to pressures below 14 kbar. The calculated Si contents of the phengite are also in accord with these natural occurrences, even though the simple phengite model used here predicts only a very small interlayer cation deficiency (1–2%) in comparison with those seen in the natural white mica (10% or more) documented by Agard *et al.* (2001). The vacancy contents contoured in Fig. 7 are intended only as a rough guide to the relative effects of temperature and bulk composition on this substitution. In the absence

**Fig. 7.** *P, T* pseudosection for average Dalradian metapelite bulk composition, ignoring melting at high temperatures. The diagram is contoured for silica content of phengite. A key feature is the disappearance of biotite with increasing pressure and decreasing temperature to form leucoschist assemblages. Biotite-absent garnet–phengite schists (common in eclogite facies terranes such as the Adula Nappe, Switzerland) imply pressures of 17 kbar and higher. g = garnet, ctd = chloritoid, car = carpholite, st = staurolite, ky = kyanite, and = andalusite, sill = sillimanite, bi = biotite, chl = chlorite.

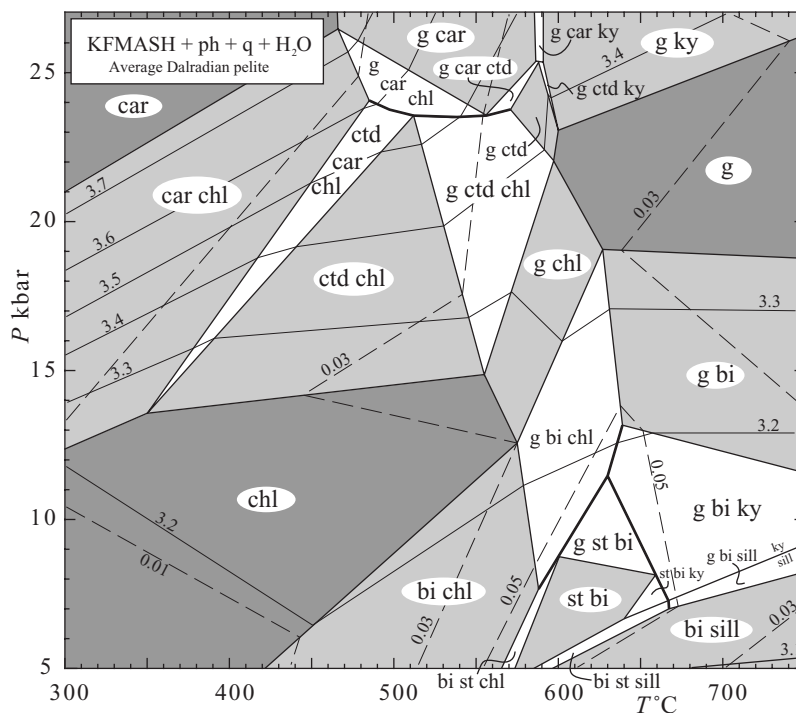
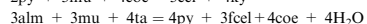
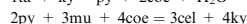
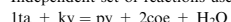


**Table 5.** Mineral data and results for average PT calculations of pyrope–coesite rock 2–39. Site distributions and end-member proportions for phengite:

Site	Element	Cations	End-member	Proportion
T1	Si	0.775	mu	0.386
	Al	0.225	cel	0.539
			fcel	0.010
M1	Mg	0.006	ma	0.004
	Fe <sup>2+</sup>	0.0001	pa	0.024
	V	0.994	prl	0.018
			fmu	0.000
M2A	Al	0.445	tmu	0.012
	Fe <sup>2+</sup>	0.010	phl	0.006
	Mg	0.545		
M2B	Al	0.982		
	Fe <sup>2+</sup>	0.0001		
	Mg	0.006		
	Fe <sup>3+</sup>	0.000		
	Ti	0.012		
A	Ca	0.004		
	Na	0.024		
	K	0.954		
	V	0.018		
Activities and their uncertainties:				
	py	alm	mu	cel
a	0.880	5.80e-6	0.350	0.360 0
sd(a)/a	0.15000	1.66973	0.10007	0.12288
fcel	ta	ky	coe	
00680	0.880	1.00	1.00	
1.47059	0.10000	0	0	

Independent set of reactions used:



Average *PT* (for a(H<sub>2</sub>O) = 0.5).

Average pressure and temperature (with uncertainties), correlation coefficient and sigma(fit):

T = 721 °C, sd = 21, P = 33.2 kbar, sd = 2.0, cor = -0.519, sigfit = 0.97.

of reliable calibration data, a mixing model involving the pyrophyllite end-member (see the appendix for details) was chosen so as to introduce only a small interlayer vacancy content (< 6%), and to have only a minor effect on the phase relations in Fig. 7. Interestingly, the pyrophyllite model for vacancy substitution leads to an increase in vacancy content with temperature for the low-grade chlorite-carpholite assemblages discussed above, in contrast to the behaviour suggested by Agard *et al.* (2001). Our calculations suggest that somewhat higher interlayer vacancies may occur in more aluminous assemblages such as those with pyrophyllite at low grade and with kyanite at higher grades. If indeed all the vacancies in mica from low-grade chlorite-phengite assemblages can be attributed to pyrophyllite substitution (rather than to other possible substituents such as NH<sub>3</sub> or H<sub>2</sub>O or H<sub>3</sub>O<sup>+</sup>), then it follows from this model that typical barrovian staurolite–kyanite grade assemblages should have even higher vacancy levels than these. Of more concern perhaps is that the experimental studies involving muscovite in aluminous assemblages might need examination with a view to re-evaluation of the standard enthalpies of muscovite and paragonite. Such findings as these are of a preliminary and exploratory nature and point to further work being needed on this substitution.

## ACKNOWLEDGEMENTS

We are grateful to C. Chopin and O. Vidal for their very helpful comments, corrections and suggestions.

## REFERENCES

- Agard, P., Vidal, O. & Goffé, B., 2001. Interlayer and Si content of phengite in HP-LT carpholite-bearing metapelites. *Journal of Metamorphic Geology*, **19**, 479–496.
- Aranovich, L. Ya. & Newton, R. C., 1996. H<sub>2</sub>O activity in concentrated NaCl solutions at high pressures and temperatures measured by the brucite-periclase equilibrium. *Contributions to Mineralogy and Petrology*, **125**, 200–212.
- Atherton, M. P. & Brotherton, M. S., 1982. Major element composition of the pelites of the Scottish Dalradian. *Geological Journal*, **17**, 185–221.
- Berman, R. G., 1988. Internally-consistent thermodynamic data for minerals in the system Na<sub>2</sub>O-K<sub>2</sub>O-CaO-MgO-FeO-Fe<sub>2</sub>O<sub>3</sub>-Al<sub>2</sub>O<sub>3</sub>-SiO<sub>2</sub>-TiO<sub>2</sub>-H<sub>2</sub>O-CO<sub>2</sub>. *Journal of Petrology*, **29**, 445–522.
- Birch, F., 1966. Compressibility; elastic constants. In: *Handbook of Physical Constants, Memoir*, 97 (ed. Clark, S. P.), 97–173. Geological Society of America, Boulder.
- Brace, W. F., Scholz, C. H. & La Mori, P. N., 1969. Isothermal compressibility of kyanite, andalusite and sillimanite from synthetic aggregates. *Journal of Geophysical Research*, **74**, 2089–2098.
- Chatillon-Colinet, C., Kleppa, O. J., Newton, R. C. & Perkins, D., 1983. Enthalpy of formation of Fe<sub>3</sub>Al<sub>2</sub>Si<sub>3</sub>O<sub>12</sub> (almandine) by high temperature alkali borate solution calorimetry. *Geochimica et Cosmochimica Acta*, **47**, 439–444.
- Chatterjee, N. D. & Flux, S., 1986. Thermodynamic mixing properties of muscovite-paragonite solid solutions at high temperatures and pressures, and their geological applications. *Journal of Petrology*, **27**, 677–693.
- Chopin, C., 1981. Talc-phengite: a widespread assemblage in high-grade pelitic blueschists of the Western Alps. *Journal of Petrology*, **22**, 628–650.
- Chopin, C., 1984. Coesite and pure pyrope in high-grade blueschists of the Western Alps: a first record and some consequences. *Contributions to Mineralogy and Petrology*, **86**, 107–118.
- Chopin, C. & Schreyer, W., 1983. Magnesiochloritoid and magnesiochloritoid: Two index minerals of pelitic blueschists and their preliminary phase relations in the model system MgO-Al<sub>2</sub>O<sub>3</sub>-SiO<sub>2</sub>-H<sub>2</sub>O. *American Journal of Science*, **283A**, 72–96.
- Comodi, P., Mellini, M. & Zanazzi, P. F., 1991. Magnesiochloritoid: compressibility and high pressure structure refinement. *Physics and Chemistry of Minerals*, **18**, 483–490.
- Comodi, P. & Zanazzi, P. F., 1994. High pressure structural study of muscovite. *IMA 16th General Meeting, Pisa*, abstracts, 79–80.
- Dorogokupets, P. I., 1995. Equation of state for lambda transition in quartz. *Journal of Geophysical Research*, **100**, 8489–8499.
- Ernst, W. G., 1963. Significance of phengitic micas from low-grade schists. *American Mineralogist*, **48**, 1357–1373.
- Eugster, H. P., Albee, A. L., Bence, A. E., Thompson, J. B. & Waldbaum, D. R., 1972. The two-phase region and excess mixing properties of paragonite-muscovite crystalline solutions. *Journal of Petrology*, **13**, 147–179.
- Flux, S. & Chatterjee, N. D., 1986. Experimental reversal of the Na-K exchange reaction between muscovite-paragonite crystalline solutions and a 2 molal aqueous (Na,K) Cl fluid. *Journal of Petrology*, **27**, 665–676.
- Green, T. H. & Hellman, P. L., 1982. Fe-Mg partitioning between coexisting garnet and phengite at high pressure, and comments on a garnet-phengite geothermometer. *Lithos*, **15**, 253–266.
- Guggenheim, S., Chang, Y. H. & Koster Van Groos, A. F., 1987. Muscovite dehydroxylation: high-temperature studies. *American Mineralogist*, **72**, 537–550.
- Guidotti, C. V., Sassi, F. P., Sassi, R. & Blencoe, J. G., 1994. The effect of ferromagnesian components on the paragonite-muscovite solvus: a semiquantitative analysis based on chemical data for natural paragonite-muscovite pairs. *Journal of Metamorphic Geology*, **12**, 779–788.
- Hazen, R. M., Downs, R. T., Conrad, P. G., Finger, L. W. & Gasparik, T., 1994. Comparative compressibilities of majorite-type garnets. *Physics and Chemistry of Minerals*, **21**, 344–349.
- Hazen, R. M. & Finger, L. W., 1978. The crystal structures and compressibilities of layer minerals at high pressure. II. Phlogopite and chlorite. *American Mineralogist*, **63**, 293–296.
- Heinrich, C. A., 1982. Kyanite-eclogite to amphibolite facies evolution of hydrous mafic and pelitic rocks, Adula Nappe, Central Alps. *Contributions to Mineralogy and Petrology*, **81**, 30–38.
- Hewitt, D. A. & Wones, D. R., 1975. Physical properties of some synthetic Fe-Mg-Al trioctahedral biotites. *American Mineralogist*, **60**, 854–862.
- Höck, V., 1974. Coexisting phengite, paragonite and margarite in metasediments of the Mittlerer Hohe Tauern, Austria. *Contributions to Mineralogy and Petrology*, **43**, 261–273.
- Hodges, K. V. & Spear, F. S., 1982. Geothermometry, geobarometry and the Al<sub>2</sub>SiO<sub>5</sub> triple point at Mt. Moosilauke, New Hampshire. *American Mineralogist*, **67**, 1118–1134.
- Holland, T. J. B., 1989. The dependence of entropy on volume for silicate and oxide minerals: a review and a predictive model. *American Mineralogist*, **74**, 5–13.
- Holland, T. J. B. & Powell, R., 1990. An enlarged and updated internally consistent thermodynamic data set with uncertainties and correlations: the system K<sub>2</sub>O-Na<sub>2</sub>O-CaO-MgO-MnO-FeO-Fe<sub>2</sub>O<sub>3</sub>-Al<sub>2</sub>O<sub>3</sub>-TiO<sub>2</sub>-SiO<sub>2</sub>-C-H<sub>2</sub>O. *Journal of Metamorphic Geology*, **8**, 89–124.
- Holland, T. J. B. & Powell, R., 1998. An internally-consistent thermodynamic data set for phases of petrological interest. *Journal of Metamorphic Geology*, **16**, 309–343.
- Hoschek, G., 1995. Stability relations and Al content of tremolite and talc in CMASH assemblages with kyanite + zoisite + quartz + H<sub>2</sub>O. *European Journal of Mineralogy*, **7**, 353–362.
- Hynes, A. & Forest, R. C., 1988. Empirical garnet-muscovite geothermometry in low grade metapelites, Selwyn Range (Canadian Rockies). *Journal of Metamorphic Geology*, **8**, 89–124.
- Ivaldi, G., Catti, M. & Ferraris, G., 1988. Crystal structure at 25 and 700 °C of magnesiochloritoid from a high pressure assemblage (Monte Rosa). *American Mineralogist*, **73**, 358–364.
- Levien, L. & Prewitt, C. T., 1981. High pressure crystal structure and compressibility of coesite. *American Mineralogist*, **66**, 324–333.
- Massonne, H.-J. & Schreyer, W., 1986. High pressure syntheses and X-ray properties of white micas in the system K<sub>2</sub>O-MgO-Al<sub>2</sub>O<sub>3</sub>-SiO<sub>2</sub>-H<sub>2</sub>O. *Neues Jahrbuch für Mineralogie Abhandlungen*, **153**, 177–215.
- Massonne, H.-J. & Schreyer, W., 1987. Phengite geobarometry based on the limiting assemblage with K-feldspar, phlogopite, and quartz. *Contributions to Mineralogy and Petrology*, **96**, 212–224.
- Massonne, H.-J. & Schreyer, W., 1989. Stability field of the high pressure assemblage talc + phengite and two new phengite barometers. *European Journal of Mineralogy*, **1**, 391–410.
- Massonne, H.-J. & Szpurka, Z., 1997. Thermodynamic properties of white micas on the basis of high-pressure experiments in the systems K<sub>2</sub>O-MgO-Al<sub>2</sub>O<sub>3</sub>-SiO<sub>2</sub>-H<sub>2</sub>O and K<sub>2</sub>O-FeO-Al<sub>2</sub>O<sub>3</sub>-SiO<sub>2</sub>-H<sub>2</sub>O. *Lithos*, **41**, 229–250.
- Nelson, D. O. & Guggenheim, S., 1993. Inferred limits to the oxidation of Fe in chlorites: a high-temperature single-crystal X-ray study. *American Mineralogist*, **78**, 1197–1207.
- Pascal, M. L. & Roux, J., 1985. K-Na exchange equilibria between muscovite-paragonite solid solution and hydrothermal chloride solution. *Mineralogical Magazine*, **49**, 515–521.
- Pavese, A., Ferraris, G., Pischedda, V. & Ibberson, R., 1999. Tetrahedral order in phengite 2M<sub>1</sub> upon heating, from powder neutron diffraction, and thermodynamic consequences. *European Journal of Mineralogy*, **11**, 309–320.

- Pavese, A., Ferraris, G., Prencipe, M. & Ibberson, R., 1997. Cation site ordering in phengite 3T from the Dora-Maira Massif (Western Alps): a variable-temperature neutron powder diffraction study. *European Journal of Mineralogy*, **9**, 1183–1190.
- Pawley, A. R., Redfern, S. A. T. & Wood, B. J., 1995. Thermal expansivities and compressibilities of hydrous phases in the system MgO–SiO<sub>2</sub>–H<sub>2</sub>O: talc, phase A and 10-Å phase. 340. *Contributions to Mineralogy and Petrology*, **122**, 301–307.
- Powell, R. & Evans, J. A., 1983. A new geobarometer for the assemblage biotite-muscovite-chlorite-quartz. *Journal of Metamorphic Geology*, **1**, 331–336.
- Powell, R. & Holland, T. J. B., 1994. Optimal geothermometry and geobarometry. *American Mineralogist*, **79**, 120–133.
- Powell, R., Holland, T. J. B. & Worley, B., 1998. Calculating phase diagrams with THERMOCALC: methods and examples. *Journal of Metamorphic Geology*, **16**, 577–588.
- Ralph, R. L., Finger, L. W., Hazen, R. M. & Ghose, S., 1984. Compressibility and crystal structure of andalusite at high pressure. *American Mineralogist*, **69**, 513–519.
- Rao, B. & Johannes, W., 1979. Further data on the stability of staurolite + quartz. *Neues Jahrbuch für Mineralogie Monatshefte*, 437–447.
- Robie, R. A., Bethke, P. E. & Beardsley, K. M., 1967. Selected X-ray crystallographic data, molar Volumes, and densities of minerals and related substances. *United States Geological Survey Bulletin*, **1248**, 87p.
- Robie, R. A. & Hemingway, B. S., 1995. Thermodynamic properties of minerals and related substances at 298.15 K and 1 bar (10<sup>5</sup> Pascals) pressure and at higher temperatures. *United States Geological Survey Bulletin*, **2131**, 461p.
- Rosenfeld, J. L., Thompson, J. B., Zen, E.-an, 1958. Data on coexistent muscovite and paragonite. *Bulletin of the Geological Society of America*, **69**, 1637.
- Roux, J. & Hovis, G. L., 1996. Thermodynamic mixing models for muscovite-paragonite solutions based on solution calorimetric and phase equilibrium data. *Journal of Petrology*, **37**, 1241–1254.
- Sato, Y., Akaogi, M. & Akimoto, S., 1978. Hydrostatic compression of the synthetic garnets pyrope and almandine. *Journal of Geophysical Research*, **83**, 335–338.
- Schertl, H.-P., Schreyer, W. & Chopin, C., 1991. The pyrope-coesite rocks and their country rocks at Parigi, Dora Maira Massif, Western Alps: detailed petrography, mineral chemistry and PT-path. *Contributions to Mineralogy and Petrology*, **108**, 1–21.
- Schmidt, M. W., Dugnani, M. & Artioli, G., 2001. Synthesis and characterization of white micas in the join muscovite-aluminoceladonite. *American Mineralogist*, **86**, 555–565.
- Schreyer, W. & Seifert, F., 1969. High pressure phases in the system MgO–Al<sub>2</sub>O<sub>3</sub>–SiO<sub>2</sub>–H<sub>2</sub>O. *American Journal of Science*, **267A**, 407–443.
- Skinner, B. J., 1966. Thermal expansion. In: *Handbook of Physical Constants, Memoir*, 97 (ed. Clark, S. P.), 75–96. Geological Society of America, Boulder.
- Smyth, J. R., Jacobsen, S. D., Swope, R. J., Angel, R. J., Arlt, T., Domanik, K. & Holloway, J. R., 2000. Crystal structures and compressibilities of synthetic 2M<sub>1</sub> and 3T micas. *European Journal of Mineralogy*, **12**, 955–963.
- Takeda, H. & Morosin, B., 1975. Comparison of observed and predicted structural parameters of mica at high temperatures. *Acta Crystallographica, B*, **31**, 2444–2452.
- Trotet, F., Vidal, O. & Jolivet, L., 2001. Exhumation of Syros and Sifnos metamorphic rocks (Cyclades, Greece). New constraints on the P-T paths. *European Journal of Mineralogy*, **13**, 901–920.
- Velde, B., 1965. Phengite micas: synthesis, stability, and natural occurrence. *American Journal of Science*, **263**, 886–913.
- Vidal, O., Goffé, B., Bousquet, R. & Parra, T., 1999. Calibration and testing of an empirical chloritoid-chlorite thermometer and thermodynamic data for daphnite. *Journal of Metamorphic Geology*, **17**, 25–39.
- Vidal, O. & Parra, T., 2000. Exhumation paths of high-pressure metapelites obtained from local equilibria for chlorite-phengite assemblages. *Geological Journal*, **35**, 139–161.
- Viswanathan, K. & Seidel, E., 1979. Crystal chemistry of Fe-Mg Carpholites. *Contributions to Mineralogy and Petrology*, **70**, 41–47.
- Waters, D. J. & Martin, H. N., 1993. Geobarometry in phengite-bearing eclogites. *Terra Abstracts*, **5**, 410–411.
- Winter, J. K. & Ghose, S., 1979. Thermal expansion and high-temperature crystal chemistry of the Al<sub>2</sub>SiO<sub>5</sub> polymorphs. *American Mineralogist*, **64**, 573–586.

Received 12 October 2001; revision accepted 1 April 2002.

## APPENDIX

Application of the models derived in this study to natural phengitic micas involves incorporating elements outside the NKF MASH system as well as a method of estimating ferric iron.

(1) *Ferric iron estimation.* There is no single reliable method available, and so the assumption is made that the sum of octahedral and tetrahedral cations is 6.05 (on an 11 oxygen basis). This arbitrary (but reasonable) assumption allows for a small amount of trioctahedral component, and is based on a survey of wet chemical analyses. As an upper limit, no more than 70% of the total iron is allowed to

be converted into ferric iron. As a result, in what follows the fcel end-member activities are likely to be rather uncertain.

(2) *Enlarged activity model.* There are many ways of projecting the larger natural system into a model NKF MASH system, and the method advocated here is to take the full system, allocate cations to sites, and then derive a set of end-members to apportion from the analysis. We will ignore Cr and Mn (which can be included by extending the model below), and treat phengite as being made up from the following nine end-members (Table A1, in which V denotes a site vacancy).

The nine end-member model requires a set of eight composition variables to describe it. The following 8 variables constitute an independent set:

Table A1.

	A	M1	M2A	M2B	T1	T2
mu	K	V	Al	Al	Al Si	Si <sub>2</sub>
cel	K	V	Mg	Al	Si Si	Si <sub>2</sub>
fcel	K	V	Fe <sup>2+</sup>	Al	Si Si	Si <sub>2</sub>
pa	Na	V	Al	Al	Al Si	Si <sub>2</sub>
ma	Ca	V	Al	Al	Al Al	Si <sub>2</sub>
fmu	K	V	Al	Fe <sup>3+</sup>	Al Si	Si <sub>2</sub>
tmu	K	V	Al	Ti	Al Al	Si <sub>2</sub>
pri	V	V	Al	Al	Si Si	Si <sub>2</sub>
phl	K	Mg	Mg	Mg	Al Si	Si <sub>2</sub>

$$x = \text{Fe}^{2+}/(\text{Fe}^{2+} + \text{Mg})$$

$$y = 2 - \text{Si}/2$$

$$z = 1 - \text{Na} - \text{K} - \text{Ca}$$

$$na = \text{Na}$$

$$ca = \text{Ca}$$

$$t = \text{Ti}$$

$$f = \text{Fe}^{3+}$$

$$p = \text{Si} + \text{Ti} + \text{Al} + \text{Fe}^{2+} + \text{Fe}^{3+} + \text{Mg} - 6.0$$

In the above  $x$  is the bulk mica  $\text{Fe}^{2+}/(\text{Fe}^{2+} + \text{Mg})$  ratio, and  $p$  is the trioctahedral excess. Note that where  $p > 0$ , there will be  $\text{Fe}^{2+}$  and Mg on both the M1 and the M2B site (see below).

The site fractions are then expressed in terms of the eight variables.

$$\begin{aligned} X_{\text{Si},\text{T1}} &= 1 - y \\ X_{\text{Al},\text{T1}} &= y \\ X_{\text{Al},\text{M2B}} &= 1 - f - t - p \\ X_{\text{Fe3},\text{M2B}} &= f \\ X_{\text{Ti},\text{M2B}} &= t \\ X_{\text{Fe2},\text{M2B}} &= xp \\ X_{\text{Mg},\text{M2B}} &= (1 - x)p \\ X_{\text{Al},\text{M2A}} &= y + z - t - ca - p \\ X_{\text{Fe2},\text{M2A}} &= x(1 - 2y - z + t + ca + p) \\ X_{\text{Mg},\text{M2A}} &= (1 - x)(1 - 2y - z + t + ca + p) \\ X_{\text{V},\text{M1}} &= 1 - p \\ X_{\text{Fe2},\text{M1}} &= xp \\ X_{\text{Mg},\text{M1}} &= (1 - x)p \\ X_{\text{V},\text{A}} &= z \\ X_{\text{Na},\text{A}} &= na \\ X_{\text{K},\text{A}} &= 1 - z - na - ca \\ X_{\text{Ca},\text{A}} &= ca \end{aligned}$$

Ideal activities for the major six end-members are given by the usual mixing-on-sites expressions:

$$\begin{aligned} a_{\text{mu}}^{\text{ideal}} &= 4X_{\text{K}}^{\text{A}}X_{\text{V}}^{\text{M1}}X_{\text{Al}}^{\text{M2A}}X_{\text{Al}}^{\text{M2B}}X_{\text{Al}}^{\text{T1}}X_{\text{Si}}^{\text{T1}} \\ a_{\text{pa}}^{\text{ideal}} &= 4X_{\text{Na}}^{\text{A}}X_{\text{V}}^{\text{M1}}X_{\text{Al}}^{\text{M2A}}X_{\text{Al}}^{\text{M2B}}X_{\text{Al}}^{\text{T1}}X_{\text{Si}}^{\text{T1}} \\ a_{\text{cel}}^{\text{ideal}} &= X_{\text{K}}^{\text{A}}X_{\text{V}}^{\text{M1}}X_{\text{Mg}}^{\text{M2A}}X_{\text{Al}}^{\text{M2B}}(X_{\text{Si}}^{\text{T1}})^2 \\ a_{\text{fcel}}^{\text{ideal}} &= X_{\text{K}}^{\text{A}}X_{\text{V}}^{\text{M1}}X_{\text{Fe}}^{\text{M2A}}X_{\text{Al}}^{\text{M2B}}(X_{\text{Si}}^{\text{T1}})^2 \\ a_{\text{ma}}^{\text{ideal}} &= X_{\text{Ca}}^{\text{A}}X_{\text{V}}^{\text{M1}}X_{\text{Al}}^{\text{M2A}}X_{\text{Al}}^{\text{M2B}}(X_{\text{Al}}^{\text{T1}})^2 \\ a_{\text{prl}}^{\text{ideal}} &= X_{\text{V}}^{\text{A}}X_{\text{V}}^{\text{M1}}X_{\text{Al}}^{\text{M2A}}X_{\text{Al}}^{\text{M2B}}(X_{\text{Si}}^{\text{T1}})^2 \end{aligned}$$

and the proportions of the end-members are given as

$$\begin{aligned} p_{\text{pa}} &= na \\ p_{\text{prl}} &= z \\ p_{\text{ma}} &= ca \\ p_{\text{tmu}} &= t \\ p_{\text{fmu}} &= f \\ p_{\text{phl}} &= p \\ p_{\text{mu}} &= 2y - na - 2ca - 2t - f - p \\ p_{\text{fcel}} &= x(1 + 3p + t + ca - 2y - z) \\ p_{\text{cel}} &= (1 - x)(1 + 3p + t + ca - 2y - z) - 3p \end{aligned}$$

The non-ideal contributions to the activity are given by the van Laar model expressions for the activity coefficient (Holland & Powell,

**Table A2.**  $W_{ij}$  parameters for the different binary constituents.

	pa	ma	cel	fcel	prl
mu	*	30	0.2P	0.2P	20 + 0.2P
pa		14.5	52	52	20 + 0.2P
ma			30	30	30 + 0.2P
cel				0	25 + 0.2P
fcel					25 + 0.2P

\*  $W_{\text{pa-mu}} = 10.12 + 0.0034T + 0.353P$ .

2002, in prep.):

$$RT \ln \gamma_l = - \sum_i \sum_{j>i} q_i q_j W_{ij}^*$$

where  $q_i = 1 - \Phi_i$  when  $i = l$  and  $q_i = -\Phi_i$  when  $i \neq l$ ,  $\Phi_i = x_i V_i / (\sum_i x_i V_i)$  and  $W_{ij}^* = W_{ij} 2V_i (V_i + V_j)$ . Thus, as an example, in a ternary solution the activity coefficient of component 1 is given as

$$\begin{aligned} RT \ln \gamma_1 &= (1 - \Phi_1) \Phi_2 \frac{2V_1}{V_1 + V_2} W_{12} \\ &+ (1 - \Phi_1) \Phi_3 \frac{2V_1}{V_1 + V_3} W_{13} - \Phi_2 \Phi_3 \frac{2V_1}{V_2 + V_3} W_{23} \end{aligned}$$

where

$$\Phi_1 = \frac{x_1 V_1}{x_1 V_1 + x_2 V_2 + x_3 V_3}, \quad \Phi_2 = \frac{x_2 V_2}{x_1 V_1 + x_2 V_2 + x_3 V_3}$$

and

$$\Phi_3 = \frac{x_3 V_3}{x_1 V_1 + x_2 V_2 + x_3 V_3}$$

The  $V_i$  values for all the potassic end-members (mu, cel, fmu, tmu) are taken as the same ( $V_i = 0.63$ ) whereas  $V_{\text{ma}}$  is taken to be the same as  $V_{\text{pa}}$  (0.37) and  $V_{\text{prl}}$  is taken as 0.50. Thus the asymmetry present is taken as reflecting primarily the size differences between Na (and Ca) and K.

The  $W_{ij}$  parameters for the different binary constituents are given in Table A2.

The values above for pa–mu–cel–fcel are based on the results of this work; others are estimated as follows:  $W_{\text{pa-ma}} = 14.5$  kJ from the coexisting micas of Höck (1974) and the  $W$ 's involving pa, ma and prl with other end-members are set to values which allow for some solvus-related non-ideality. The  $W$  terms involving prl were assigned such that only small amounts of prl are generated in assemblages in Fig. 7, keeping in mind the fact that solution of mu towards prl appears to be greater than solution of cel towards prl at low grade (Agard *et al.*, 2001). Thus  $W_{\text{cel-prl}}$  and  $W_{\text{fcel-prl}}$  are both larger than  $W_{\text{mu-prl}}$ ; the pressure dependence (0.2P) is assumed to be the same as in the mu–cel binary. All other binary coefficients are set to zero. These arbitrary assignments will need to be modified as more information becomes available. In natural phengite the proportions of end-members ma, prl, fmu and tmu are often quite small (although prl might be important under some conditions) and so uncertainties in these non-ideal terms will not greatly affect the activities of the major end-members mu, pa, cel and fcel.